Chapter 1

Tomography in the tau domain

INTRODUCTION AND SUMMARY

Seismic tomography is a non-linear problem. A standard technique for dealing with this non-linearity is to iteratively assume a linear relation between the change in slowness and the change in travel times (Biondi, 1990; Etgen, 1990) and then re-linearize around the new model. In ray based methods, this amounts to assuming stationary ray paths and reflection locations to construct a back projection operator (Stork and Clayton, 1991). The change in this back projection operator from non-linear iteration to non-linear iteration can be thought of as an important second order effect.

Unfortunately, the conventional linearization has difficulties coping with the coupled relationship between reflector position and velocity (Al-Chalabi, 1997; Tieman, 1995). We can avoid some of the problems caused by this connection by transforming the problem into vertical-traveltime (tau) coordinate space (τ,x'). In the tau domain, reflector position is less sensitive to velocity changes. This modified coordinate system still allows for complex velocity structures, but significantly reduces the map migration term in tomography (Biondi et al., 1997, 1998b).

In this chapter I begin by deriving a ray-based projection operator in the depth domain. I then perform an analogous derivation in the tau domain. I show that the corresponding tau back projection operator is less sensitive to the initial velocity estimate than its depth counterpart. I finish the chapter by applying and comparing tau-space and depth-space tomography to a simple anticline model.

RAY BASED TOMOGRAPHY IN DEPTH

In tomography we linearize around an initial estimate of the slowness field. In ray based tomography the linearization assumption means we have to assume stationary raypaths. Using this assumption, in 2-D, we can write an equation for the traveltime along a ray as:

$$t = \int_{\mathbf{L}} s(z,x)dl, \tag{1.1}$$

where $s(z,x)$ is the slowness field, t is the measured travel time, and we integrate over the raypath ($\mathbf{L}$). In discrete space, we will approximate the continuous function as a series of straight ray segments through constant slowness. We rewrite equation (1.1) in terms of these ray segments as:

$$\widetilde{dt} = \sqrt{\left(\widetilde{dz}\widetilde{S}\right)^2 + \left(\widetilde{dx}\widetilde{S}\right)^2}, \tag{1.2}$$

where $\widetilde{dt}$ is the travel time of the ray segment, $\widetilde{S}$ is the slowness at the ray segment location, $\widetilde{dx}$ and $\widetilde{dz}$ are the change in x and z along the segment. We can take the derivative with respect to slowness:

$$\frac{d(\widetilde{dt})}{ds} = \sqrt{\widetilde{dz}^2 + \widetilde{dx}^2}\frac{d\widetilde{S}}{ds} \tag{1.3}$$

and end up with a linear relationship between the change in slowness and a change in the traveltime for that ray segment. We can use (1.3) as the basis for a linear operator $\mathbf{T_{z,ray}}$ which relates changes in the slowness field $\Delta\mathbf{s}$ to errors in the traveltimes $\Delta\mathbf{t}$,

$$\Delta\mathbf{t} = \mathbf{T_{z,ray}}\Delta\mathbf{s}. \tag{1.4}$$

If we were doing a transmission tomography problem, such as medical imaging or cross well seismology, we would have all we need to invert for a new slowness model. Unfortunately, in reflection tomography, there is an added unknown: the actual point where the ray reflects.

Any error in the traveltime can be accounted for by either perturbing the slowness model or by moving the reflector. One solution to this coupled relationship is to reformulate the problem in terms of both reflector movement $\Delta\mathbf{r}$ and slowness changes $\Delta\mathbf{s}$ obtaining a new objective function Q,

$$Q(\Delta\mathbf{s}, \Delta\mathbf{r}) = \|\Delta\mathbf{t} - \mathbf{T_{z,ray}}\Delta\mathbf{s} - \mathbf{R}\Delta\mathbf{r}\|^2 \tag{1.5}$$

or more conveniently, in terms of the fitting goals

$$\begin{aligned} \Delta\mathbf{t} &\approx \mathbf{T_{z,ray}}\Delta\mathbf{s} \\ \Delta\mathbf{t} &\approx \mathbf{R}\Delta r, \end{aligned} \tag{1.6}$$

where $\mathbf{R}$ is an operator that relates reflector movement to changes in traveltime. To find $\mathbf{R}$ let's consider a ray reflecting at angle θ, at 'A' (Figure 1.1). Snell's law must be obeyed at the updated, along with the initial, raypaths so it is natural to assume the the reflector moves dr normal to its initial position. Simple geometry demonstrates that the increase in the ray length due to dr is $dr\cos\theta$. We can convert the change in length to a change in travel time by multiplying by the local slowness s_{ref}. If we account for both the incident and reflector ray we end up with the linear relationship for a ray between the change in reflector position dr and the change in traveltime for the ray dt,

$$dt = 2s_{\text{ref}}dr\cos\theta. \tag{1.7}$$

Instead of directly inverting for reflector movement and slowness a common solution was to handle the slowness/reflector position coupling by freezing one component (such as reflector position) inverting for the other and then reversing the procedure. This approach has a tendency to be unstable for large reflector movements. As a result, van Trier (1990) and Stork and Clayton (1991) proposed avoiding inverting directly for the reflector position by introducing a new operator, $\mathbf{H}$, that maps reflector movement to $\Delta\mathbf{s}$, and changing the reflector movement tomography operator to:

$$\mathbf{T_{z,ref}} = \mathbf{RH}. \tag{1.8}$$

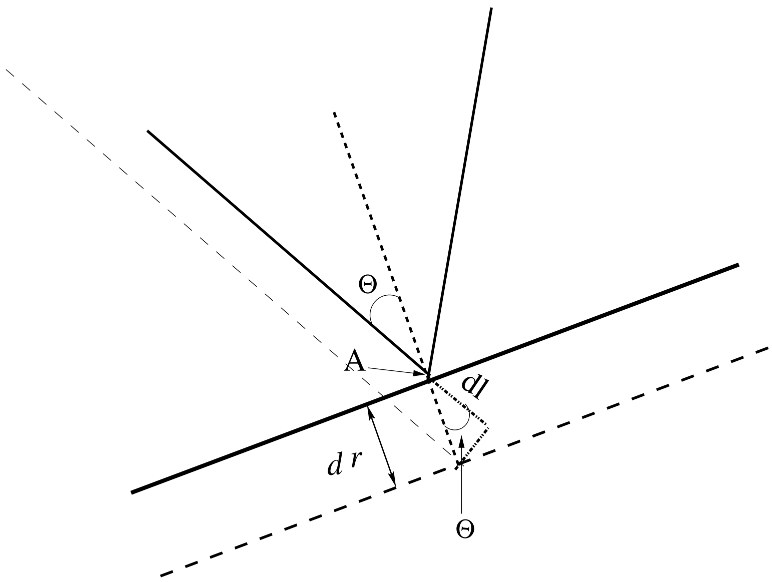

Figure 1.1: Given the initial ray path (solid lines) the change in the raypath length is $\cos\theta$ times the change in the reflector position dr. $\boxed{\text{tau-dl}}$ [NR]

As mentioned earlier, the reflector movement is normal to the reflector at the reflection point. Therefore, we approximate the change in reflector position as function of how much the slowness field changes along a ray whose takeoff angle is normal to the reflector (the zero offset ray). The arrival time at zero offset is independent of velocity. Therefore, we can write an expression between the initial ray and the ray through the updated medium,

$$
\begin{aligned}
l_{\text{new}} s_{\text{rms,new}} = t &= l s_{\text{rms}} \\
(l + dl)(s_{\text{rms}} + ds_{\text{rms}}) &= l s_{\text{rms}},
\end{aligned} \tag{1.9}
$$

where l is the length of the zero offset ray through the initial medium, s_{rms} is the RMS slowness of the media along the ray, and $s_{\text{rms,new}}$ and l_{new} are the same two quantities through the updated medium. If we ignore the second order term we end up with the expression,

$$
\frac{dl}{ds_{\text{rms}}} = -\frac{l}{s_{rms}}. \tag{1.10}
$$

If we consider each ray segment independently we end up with

$$
\frac{\widetilde{dr}}{ds} \approx -\frac{dl}{\widetilde{S}} \frac{d\widetilde{S}}{ds}. \tag{1.11}
$$

Combining the two portions of the tomography operator (Figure 1.2) we get the complete tomography operator relating slowness changes to traveltime errors,

$$\Delta \mathbf{t} \approx \left(\mathbf{T_{z,ref}} - \mathbf{T_{z,ray}}\right) \Delta \mathbf{s}. \tag{1.12}$$

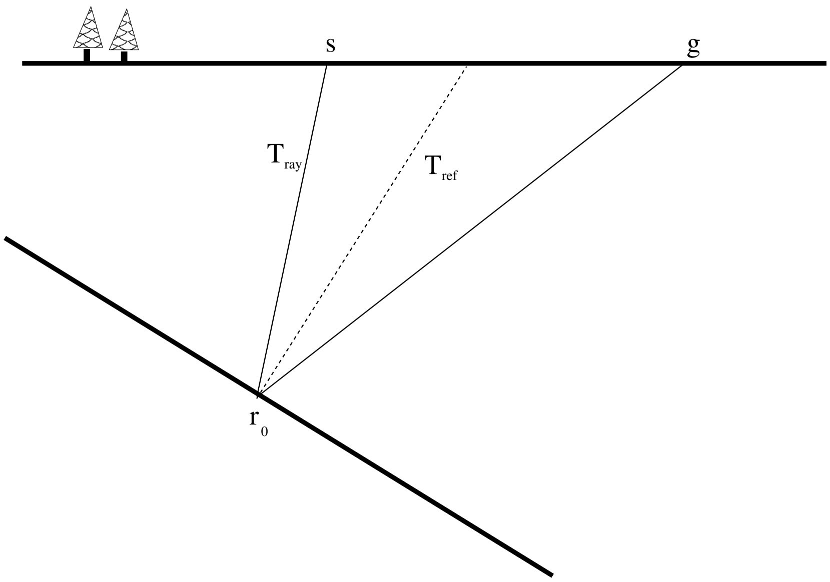

Figure 1.2: The two portions of the back projection operator for a given offset, common reflection point (CRP), and reflector position. $\mathbf{T_{ray}}$ is the ray-pair from the source $\mathbf{s}$ to the reflection point $\mathbf{r_0}$ to the receiver $\mathbf{g}$. $\mathbf{T_{ref}}$ is the raypath that is normal to the reflector at $\mathbf{r_0}$. tau-schematic [NR]

RAY BASED TOMOGRAPHY IN TAU

One of the major difficulties with depth tomography is that the reflectors may be significantly mispositioned. To illustrate this fact I constructed a synthetic model (Figure 1.3). The model is an anticline with seven reflectors. The top five reflectors are within the anticline structure. The last two, a flat reflector and a dipping reflector, are below the anticline. Positioning the two bottom reflectors correctly is the imaging challenge. For added difficulty there is a low velocity layer between the second and third reflector. The model was used to do acoustic wave modeling, with the resulting dataset having 40 meter common midpoint (CMP) spacing and 60 offsets spaced 80 meters apart. If the initial estimation of the slowness is the $s(z)$ function from outside the anticline, the migrated reflector positions are pulled up due to using too low a velocity within the anticline (Figure 1.4). The reflector mispositioning causes significant errors in the linearized tomography problem. For example, if we compare a set of true raypaths (Figure 1.5) versus the estimated raypaths, we can see that we are back projecting the moveout errors to the wrong positions in the slowness model. Another way to think about it is that the linear approximation, equation (**??**) is poor, causing us to have to take smaller step sizes per non-linear iteration, and increasing the chance that we will get stuck in local minima or maxima.

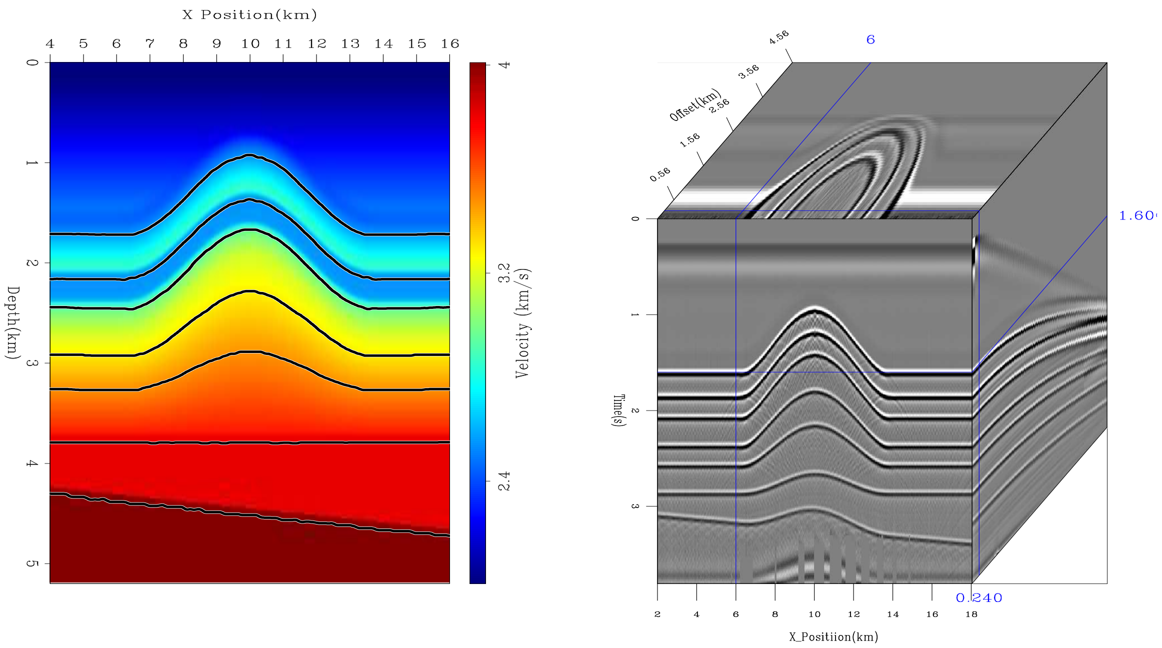

Figure 1.3: Left panel is the synthetic velocity model with seven reflectors spanning the anticline. The right panel shows the data generated from this model. Some modeling artifacts can be seen at 3.8 seconds below the anticline. $\boxed{\text{tau-synth-model}}$ [ER,M]

When doing time domain velocity analysis, reflector mispositioning is not as much of a problem. Reflector positioning in depth is done in two stages (Hubral, 1977; Larner et al., 1981). The first step is to find the velocity, v_{rms}, that best focuses the data. This can be

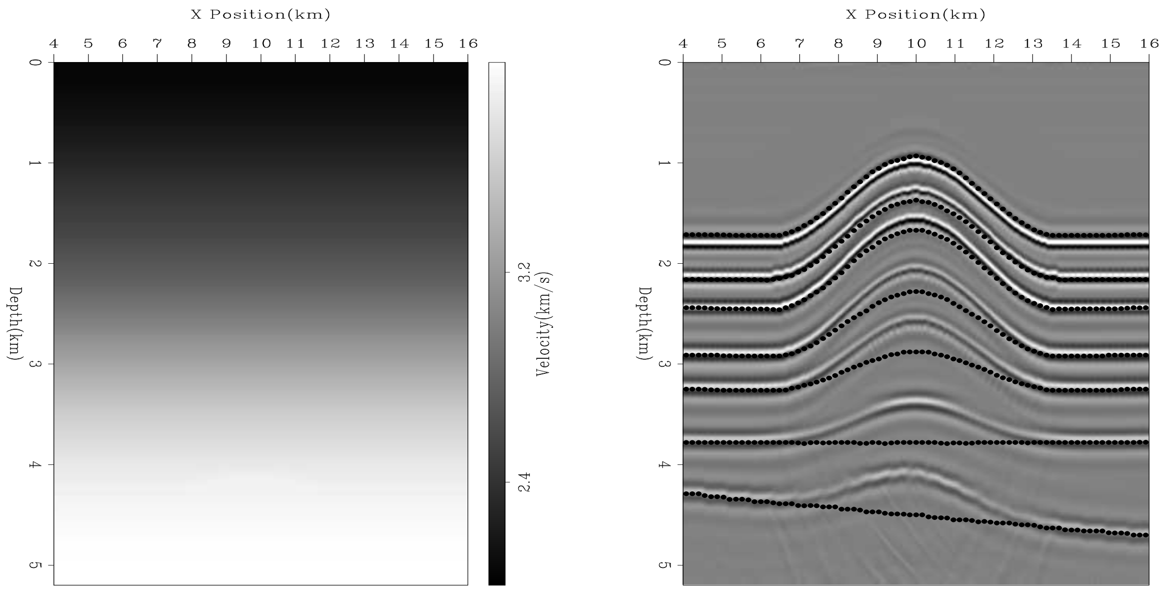

Figure 1.4: Left panel is the initial guess at the velocity function, the right panel shows the zero offset ray parameter reflector position using this migration velocity. The correct reflector positions are shown as '*'. Note that reflectors are significantly mispositioned, particularly the bottom two reflectors. tau-mig0 [ER,M]

relatively easier in time because reflector position is much less effected by velocity. After $v_{\rm rms}$ has been estimated, the reflectors are mapped in depth using a velocity function, sometimes different than $v_{\rm rms}$. The disadvantage of time domain methods is that they cannot accurately define wave behavior in complex media.

The tau domain offers a good alternative that combines the best of both depth and time velocity analysis. The tau, or vertical travel time, domain is defined by the transform

$$\tau(z,x) = \int_0^z 2s(z',x)dz' \tag{1.13}$$

$$x'(z,x) = x. \tag{1.14}$$

In this domain, flat reflectors are independent of the slowness field and dipping reflector movement is much more limited (Figure 1.6). Additionally, the coordinate transform has not diminished the ability to handle complex propagation behavior.

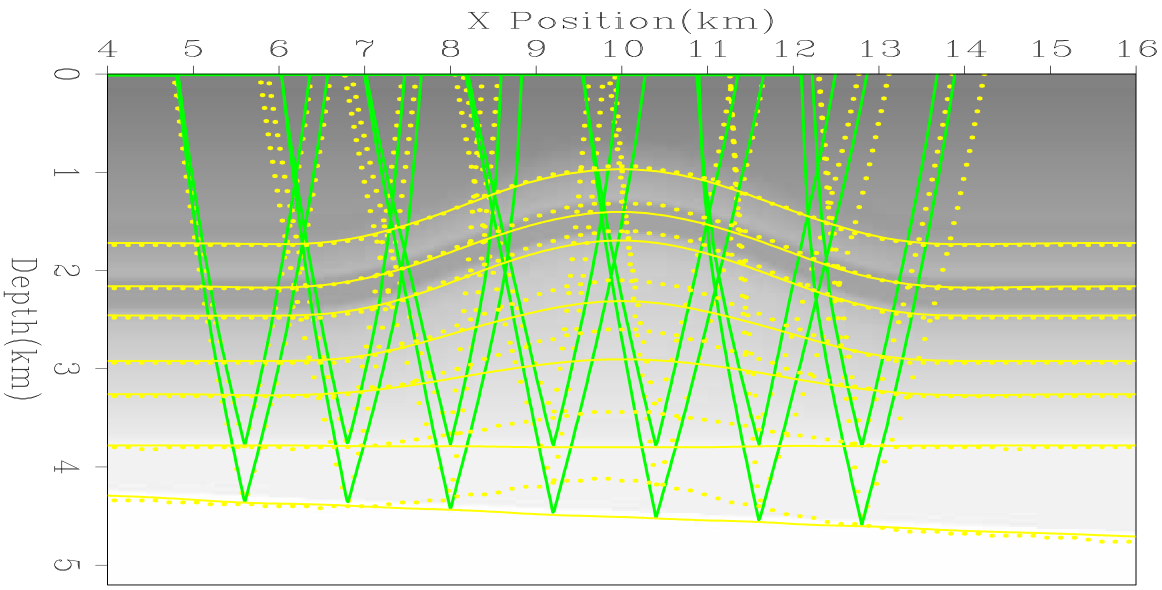

Figure 1.5: The solid lines show raypaths through the correct velocity and the correct reflector position. The dashed lines are raypaths through the initial model and the initial reflector positions. Note that the estimated raypaths have significant error, therefore the tomography operator will have significant error. $\boxed{\text{tau-rays}}$ [CR,M]

Tau operator

In order to perform tomography in the tau domain, we must find an operator equivalent to the depth domain operator (1.12) in the tau domain. This amounts to applying some simple coordinate transforms to the already derived depth equations. We will start from the relationship for a single ray segment, equation (1.2):

$$\widetilde{dt} = \sqrt{\left(\widetilde{dz}\widetilde{S}\right)^2 + \left(\widetilde{dx}\widetilde{S}\right)^2} \tag{1.15}$$

where $\widetilde{\_}$ represents a ray segment quantity.

By applying the chain rule to (1.13) and (1.14) we find a relationship between the derivatives:

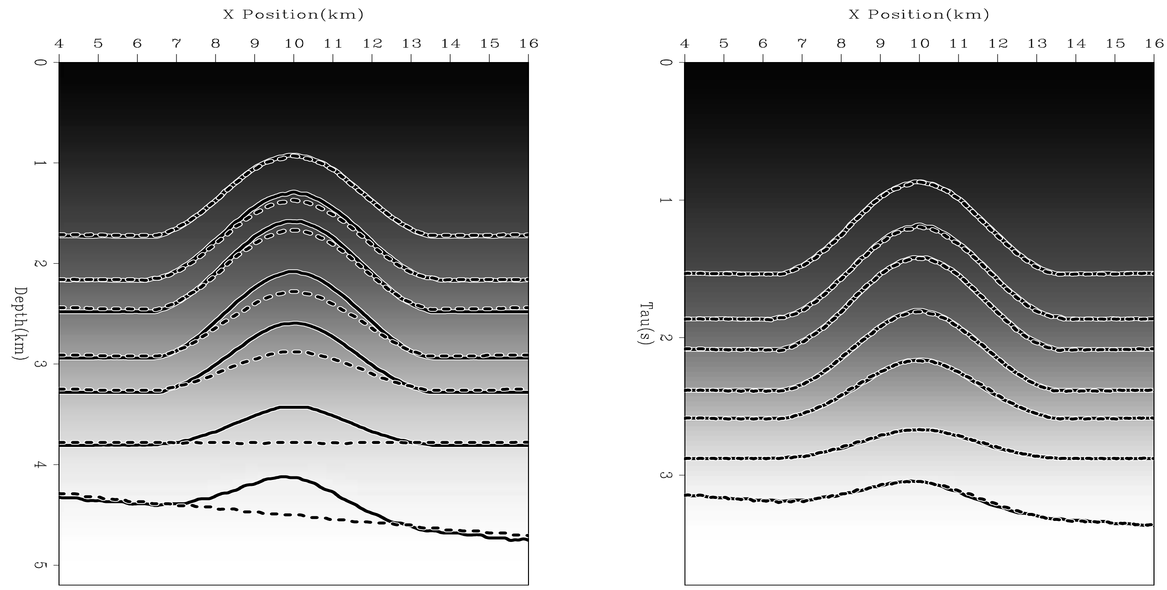

Figure 1.6: Left panel is the initial slowness model in depth. The dashed lines show the correct reflector positions, the solid lines are where the reflectors are positioned using the initial slowness model. The right panel shows the same thing in the tau domain. Note how the correct and initial reflector positions are much closer in tau. tau-tau-initial [ER,M]

$$
\begin{aligned}
\frac{\partial t}{\partial z} &= \frac{\partial t}{\partial \tau}\frac{\partial \tau}{\partial z} + \frac{\partial t}{\partial x'}\frac{\partial x'}{\partial z} = \frac{\partial t}{\partial \tau} 2s(z,x) \qquad (1.16)\\
\frac{\partial t}{\partial x} &= \frac{\partial t}{\partial x'}\frac{\partial x'}{\partial x} + \frac{\partial t}{\partial \tau}\frac{\partial \tau}{\partial x} = \frac{\partial t}{\partial x'} + \frac{\partial t}{\partial \tau}\int_0^z \frac{\partial}{\partial x}\left[2s(z',x)\right] dz'. \qquad (1.17)
\end{aligned}
$$

Rather than carrying around the integral we can define a differential mapping factor σ,

$$
\sigma(z,x) = \int_0^z \frac{\partial}{\partial x}\left[2s(z',x)\right] dz'. \qquad (1.18)
$$

The differential mapping factor has non-zero values only in areas at and below where the medium deviates from $s(z)$. For the synthetic model it is only inside the anticline (Figure 1.7).

We can use equations (1.13) and (1.14) to write a relationship between change in (z,x) and

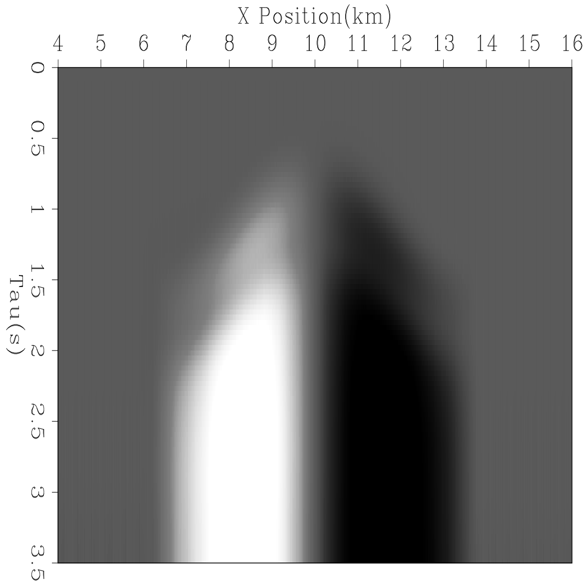

Figure 1.7: Sigma values for the synthetic model in Figure 1.6 $\boxed{\text{tau-sigma}}$ [ER]

(τ, x') space,

$$
\begin{aligned}
\widetilde{dz} &= \frac{\widetilde{d\tau}}{2\widetilde{S}} - \frac{\widetilde{\sigma}\widetilde{dx'}}{2\widetilde{S}} && (1.19)\\
\widetilde{dx} &= \widetilde{dx}. && (1.20)
\end{aligned}
$$

We apply these definitions to equation (1.15) and come up with a new definition for dt in tau space,

$$
\widetilde{dt} = \sqrt{\left(\left(\widetilde{S}\widetilde{dx'}\right)^2 + \frac{\widetilde{d\tau} - \widetilde{\sigma}\widetilde{dx'}}{2}\right)^2}. \tag{1.21}
$$

We can then take the derivative with respect to s,

$$
\frac{\widetilde{dt}}{ds} = \frac{\widetilde{S}\widetilde{dx'}^2}{\widetilde{dt}}\frac{d\widetilde{S}}{ds} - \frac{(\widetilde{d\tau} - \widetilde{dx'}\widetilde{\sigma})\widetilde{dx'}}{4\widetilde{dt}}\frac{d\widetilde{\sigma}}{ds}. \tag{1.22}
$$

Unfortunately, the operator isn't quite as simple as its depth counterpart (1.3). In this case we do not have a direct relationship between $\frac{d\widetilde{S}}{ds}$ and $\frac{\widetilde{dt}}{ds}$ because of an intermediate $\frac{d\widetilde{\sigma}}{ds}$ term. We can find a linear relationship between $\frac{d\widetilde{\sigma}}{ds}$ and $\frac{d\widetilde{S}}{ds}$ by first writing

$$
\begin{aligned}
\frac{\partial \tau}{\partial x'} &= \frac{\partial \tau}{\partial x}\frac{\partial x}{\partial x'} + \frac{\partial \tau}{\partial z}\frac{\partial z}{\partial x} \\
\frac{\partial \tau}{\partial x} &= \frac{\partial \tau}{\partial x'} - \frac{\partial}{\partial z}\int_0^z 2s(z',x)dz' \\
\sigma(z,x) &= -2s(\tau,x')\frac{\partial z}{\partial x} \\
\sigma(z,x) &= -s(\tau,x')\int_0^\tau \frac{\partial}{\partial x'}\frac{1}{s(\tau',x')}d\tau'.
\end{aligned}
\tag{1.23}
$$

We then take the partial derivative with the respect to s and evaluate along the ray segment

$$
\frac{\partial \widetilde{\sigma}}{\partial s} = \frac{\widetilde{\sigma}}{\widetilde{s}}\frac{\partial \widetilde{S}}{\partial s} - s(\tau,x')\int_0^\tau \frac{\partial^2 s(\tau',x')}{\partial x' \partial s}\partial \tau'. \tag{1.24}
$$

With this relationship (1.24) we can then create a new tomography operator in tau space:

$$
\Delta \mathbf{t} \approx \left(\mathbf{T}_{\tau,\mathbf{ref}} - \mathbf{T}_{\tau,\mathbf{ray}}\right)\Delta \mathbf{s}. \tag{1.25}
$$

OPERATOR CHANGE IN TAU VS. DEPTH

The accuracy of the linearization (**??**) is the major factor determining whether the tomography problem will converge and how many non-linear iterations it will take to get to an acceptable solution. For ray based tomography this is a function of how close the initial guess at the ray-paths is to their true locations. The smaller the difference, the more accurate the linearization, and the less likely the estimate will diverge.

By forming the tomography in τ, x' rather than z, x space, $\mathbf{T_0}$ is closer to $\mathbf{T_{nl}}$. The fundamental reason is that the data are in time rather than depth. For ray based tomography the back projection operator inherently relies on the estimates of reflector positions. In depth space, reflector positions change significantly with velocity changes. As shown earlier (Figure 1.6) changing the velocity the same amount will have very little effect in tau space. We can extend this argument to the back projection operator. In the depth space the reflectors are mispositioned and as a result we are back projecting the errors into these mispositioned locations.

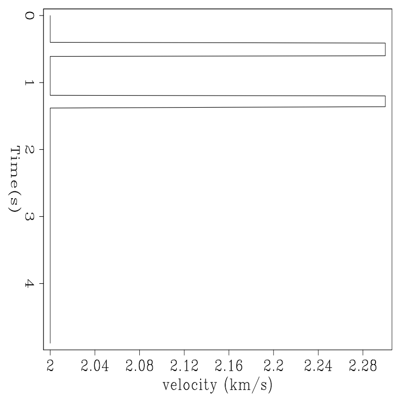

Figure 1.8: Synthetic 1-D velocity function in τ. tau-cor [ER]

In tau, the reflectors are much closer to the correct position, and the back projection will be introducing slowness change in more reasonable locations.

Simple test

To demonstrate how the tau back projection operator is less affected by the initial slowness model, I constructed a simple 1-D synthetic. The model, Figure 1.8, is composed of two 2.3 km/s zones in a constant 2 km/s background. I assume that I have correctly resolved the velocity in the lower layer. For this simple 1-D synthetic, that means that the vertical traveltime to the top and bottom of the layer boundary are correct. In depth, because we have not resolved the upper layer, we will misplace the location of the bottom high velocity zone but preserve the correct vertical travel times to the layer top and bottom. After constructing the model we found the ray that hit the reflector at 2 km depth, 2 km away from source in both τ, x and z, x space (Figure 1.9). I then built the tomography operator for both tau $\mathbf{T_{0,\tau}}$ and depth $\mathbf{T_{0,z}}$, Figure 1.10.

For comparison, I raytraced through the 'correct' velocity model in both spaces (Figure 1.11) and calculated the corresponding operators (Figure 1.12). By comparing the correct and initial operator for tau and depth, or by looking at the difference between the two operators (Figure 1.13), we can clearly see that the initial guess for the tau operator is overall better than the initial guess for the depth operator. In the upper layer, we see marginally more change in the tau operator but at the lower reflector boundaries (which move in the case of depth but

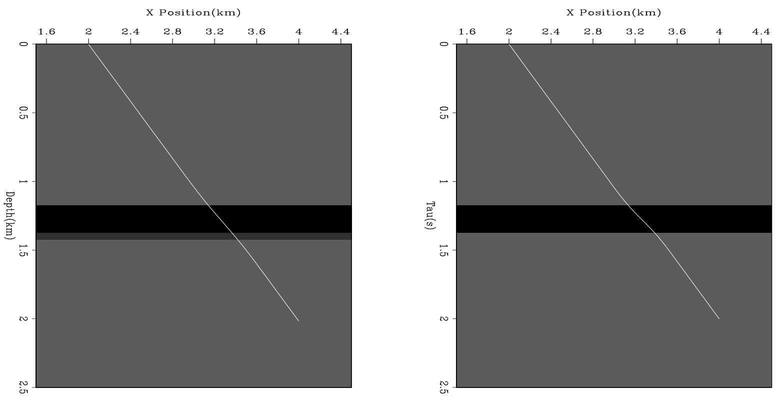

Figure 1.9: Initial guess at the velocity function overlaid by ray hitting reflector at 4 km with a half-offset of 2 km. Left panel is in depth, right panel is in tau. tau-ray.vel0 [ER,M]

remain constant in tau) we see significantly more error in depth. In addition, the change in reflector position has caused a spike in the difference panel for the depth case. Finally, the change in the tau operator is smooth, while the change in the depth operator shows dramatic jumps. The successive relinearizing has an underlying assumption that we are smoothly converging to the correct operator. In tau space, this assumption is more valid. With a more complicated model the positioning of the layer boundaries will be subject to more change, making the tau compared to depth difference even more dramatic.

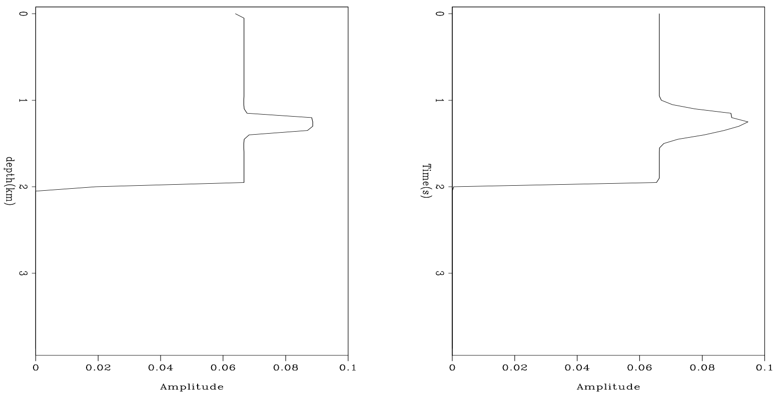

Figure 1.10: The operator calculated from the initial guess at velocity and the resulting ray paths in depth (left) and tau (right). tau-operator0 [ER,M]

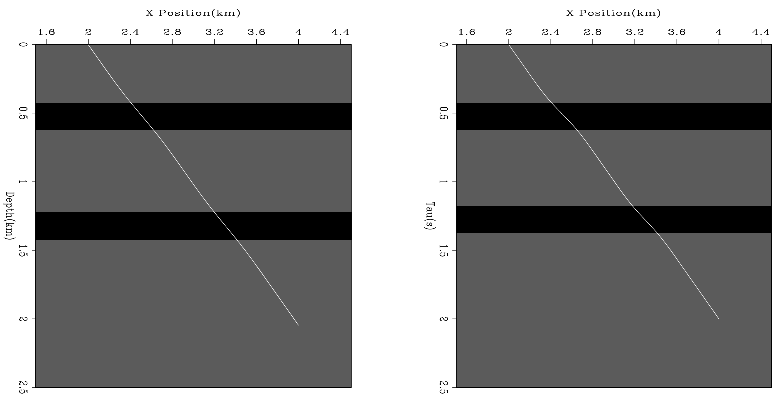

Figure 1.11: "Correct" velocity function overlaid by ray hitting reflector at 4 km with a half-offset of 2 km. Left panel is in depth, right panel is in tau. tau-ray.vel1 [ER,M]

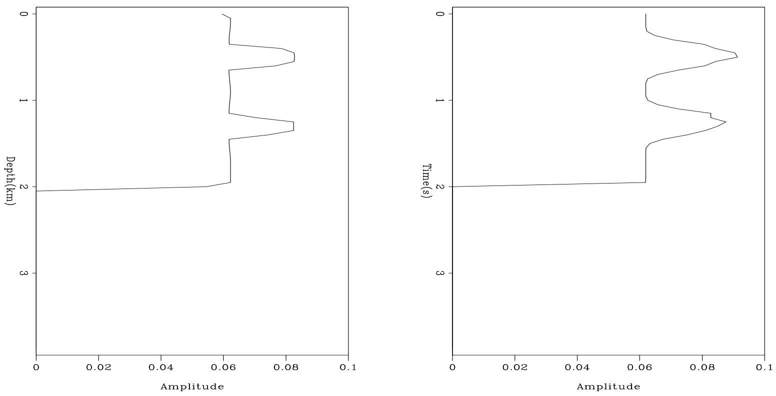

Figure 1.12: The operator calculated from the "correct" velocity and the resulting ray paths in depth (left) and tau (right). tau-operator1 [ER,M]

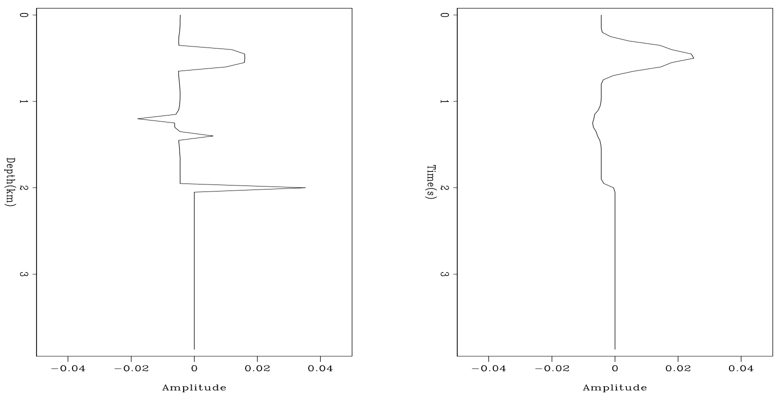

Figure 1.13: The difference between the operators calculated from the correct and the initial guess at velocity, for depth (left) and tau (right). Note the significant spikes at the reflector and at the lower layer boundary in the depth case. tau-diff [ER,M]

ANGLE DOMAIN MIGRATION TOMOGRAPHY

Wave equation angle gathers

When doing velocity analysis, general practice is to measure moveout from a relatively sparse set of CRP gathers. Kirchhoff depth migration is the preferred construction method because it can produce the sparse set of CRP gathers without needing to image the entire volume. Kirchhoff methods also have some deficiencies. The most glaring weakness of Kirchhoff methods is the difficulty in constructing the Green's function table. To construct an accurate Green's function table we must account for, and weight correctly, the multiple arrivals that occur in complex geology. Calculating and accounting for multiple arrivals adds significantly to both coding complexity and memory requirements. As a result, a single arrival is usually all that is used. Eikonal methods (Vidale, 1990; van Trier and Symes, 1991; Podvin and Lecomte, 1991; Fomel, 1997) can efficiently produce first arrivals, but in areas of complex geology the first arrival is not always the most important arrival (Audebert et al., 1997). As a result, general practice is to use expensive ray based methods. These methods still face the difficult tasks of choosing the most important arrival and correctly and efficiently interpolating the traveltime field (Sava and Biondi, 1997).

The most computationally attractive alternative to Kirchhoff methods is frequency domain downward continuation. Downward continuation has its own weaknesses. Its primary weakness is speed. Downward continuation cannot be target oriented, so full volume imaging is required. In addition, wave number domain methods cannot handle lateral variations in velocity. By migrating with multiple velocities and applying a space domain correction to the wavefield, they can do a fairly good job handling lateral variations (this migration is normally referred to as PSPI, Phase-shift plus interpolation)(Ristow and Ruhl, 1993; Gazdag and Sguazzero, 1985). Finally, downward continuation focuses the wavefield towards zero offset, making conventional moveout analysis impossible.

I can create CRP gathers where moveout analysis is possible using wave equation migration methods by changing the imaging condition (Clayton and Stolt, 1981; Prucha et al., 1999). Given a wave-field we follow the normal procedure of downward continuing the sources and receivers and extracting the image at zero time at the new recording surface. Instead of extracting the image at zero offset, we note that reflection angle θ can be evaluated by the differential equation:

$$\tan\theta = -\frac{\partial z}{\partial x_h} \tag{1.26}$$

where z is the depth, and x_h is half-offset (Sava and Fomel, 2000).

The topic of this thesis is not migration, but tomography. The tomography method could be applied with either Kirchhoff or downward continuation based migration. For me, PSPI proved to be a more attractive choice. A 2-D and 3-D PSPI algorithm was already available, where a Kirchhoff approach would have required the coding of the migration algorithm along with a suitable traveltime computation method.

Characterizing moveout errors

Tomography requires us to provide moveout errors. It is unreasonable to hand pick every reflector at every CRP gather in 2-D and inconceivable in 3-D. As a result, people have tried to find alternate methods to pick moveout errors. Clark et al. (1996) used a neural network approach to pick CRP gathers and many people have suggested seeding-based approaches to pick the gathers. Both approaches describe complicated moveouts, but they suffer from cycle skipping and have problems in areas where the S/N ratio is not high. An alternative approach is to characterize the moveout in CRP gathers by a single parameter (Etgen, 1990; van Trier, 1990). A single parameter is a much more robust estimator. It requires less human involvement (less picking and/or QA is necessary) and is less sensitive to signal to noise problems.

At early iterations a single parameter is especially valuable. All that can be resolved at early iterations are gross features. A single parameter can capture these where picking the entire CRP gather is likely to cause the inversion to be overwhelmed by small features that are not resolvable at early iterations. When we are close to the correct velocity allowing freedom in moveout behavior is desirable and beneficial.

For the tomography problem I will begin with a migrated image d at a depth z, angle θ, at CRP location x. For estimating the residual moveout in the CRP gathers by calculating semblance s in terms of some curvature parameter [1] γ

$$s(z,\gamma,x) = \frac{\left[\sum_\theta d(z+|\theta\gamma|\gamma,\theta,x)\right]^2}{n(z,x)\sum_\theta d(z+|\theta\gamma|\gamma,x)^2}, \tag{1.27}$$

where $n(z,x)$ is the number non-zero samples summed over for each semblance calculation. Figure 1.14 shows two CRP gathers overlaid are the curves corresponding to the picked γ value for each reflector. For this synthetic, the γ does a good job characterizing the moveout.

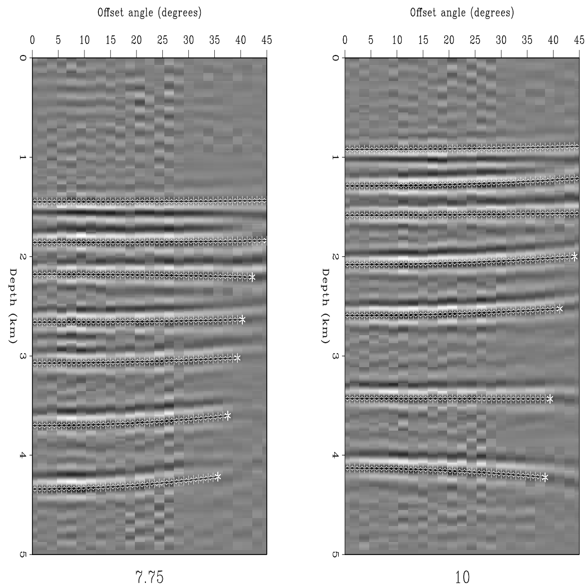

Figure 1.14: Two angle CRP gather from the anticline model (x=7.5 km and x=10.0 km) migrated with the Overlaid are the projection of the maximum γ values for each reflection. Note that the general moveout is fairly well described by γ. tau-semb-mig0 [ER,M]

For this dataset hand picking the semblance along each reflector would not be too tedious, but in 3-D it would quickly become so. As a result, I wanted to come up with a simple way for the computer to do most of the work. One option would be to just pick the maximum semblance at each location, but I can get an unrealistic, high spatial wavenumber behavior for $\gamma(x)$. When doing conventional semblance analysis we are confronted with a similar problem, that picking the maximum semblance at each time could result in an unreasonable velocity function. Clapp et al. (1998) proposed a method to avoid hand picking that still led to a reasonable velocity model. I can adapt that work by starting with a initial curvature $\boldsymbol{\gamma_0}$ equal

[1] Ottolini (1982) demonstrated that residual moveout is not hyperbolic, even in constant velocity, in angle domain gathers. For the purpose of moveout analysis for tomography the hyperbolic approximation proved to be acceptable.

to the curvature corresponding to the maximum semblance $\mathbf{W}$ at the CRP, and a derivative operator $\mathbf{D}$. I can find a smooth curvature function $\boldsymbol{\gamma}$ by setting up a simple set of regression equations

$$\begin{aligned} \mathbf{0} &\approx \mathbf{W}(\boldsymbol{\gamma_0} - \boldsymbol{\gamma}) \\ \mathbf{0} &\approx \epsilon \mathbf{D} \boldsymbol{\gamma}. \end{aligned} \tag{1.28}$$

By increasing ϵ we get smoother $\boldsymbol{\gamma}$ values while small ϵ values honor more the maximum semblance picks. Figure 1.15 shows the semblance panel for each reflector with the smooth pick overlaid.

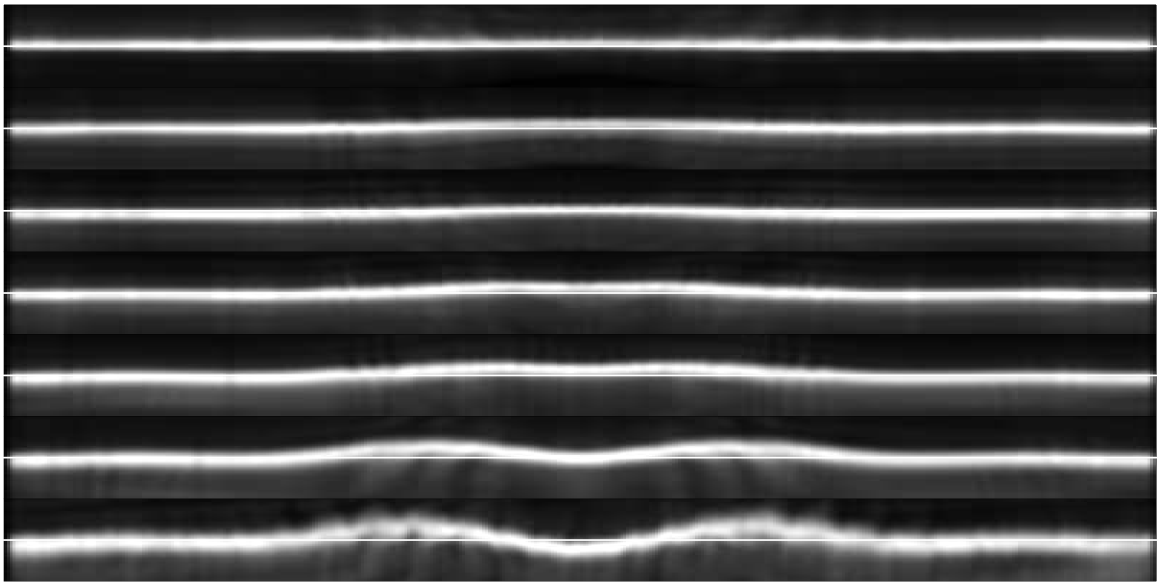

Figure 1.15: Semblance along the seven reflectors. tau-semb-mig0-ref [ER,M]

Endpoints, edge effects, and errors

To set up the tomography problem I need to cover some final details. I can convert the semblance picks back into a Δz shift by applying

$$\Delta z = \gamma \theta^2. \tag{1.29}$$

From a simple geometric argument (Figure 1.16) we can approximate errors in traveltime from the depth focusing errors (Stork, 1992). We approximate the change in ray length caused by the positioning error Δz by multiplying by the cosine of the half aperture angle θ and the cosine of the geologic dip ϕ at the reflection point 'A'. We multiply by the local slowness s_{ref} and get the final expression

$$\Delta t = 2\gamma\theta^2 s_{\text{ref}} \cos\theta \cos\phi. \tag{1.30}$$

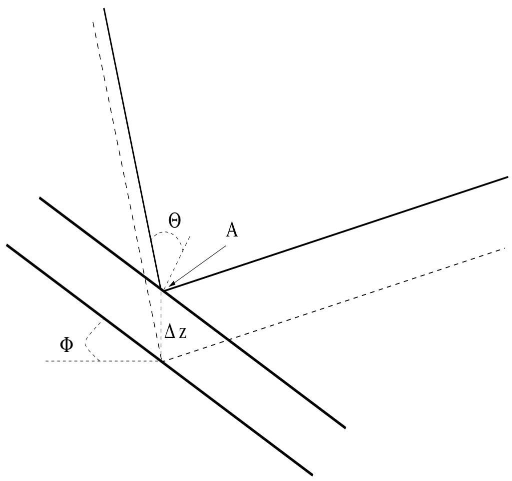

Figure 1.16: Geometric relation between a positioning error Δz and the change in ray length for a raypair reflecting at 'A' at the half aperture angle θ with a local dip ϕ. tau-ztot [NR]

In constructing the raypaths we benefit from having the CRP gathers in terms of angle. If errors were in terms of offset we would have to either

- shoot rays from every source and receiver location, and find ray pairs that obey Snell's law at the position on the reflector imaged at the offset dictated by the ray pair
- or shoot rays from the CRP locations along where the reflector is imaged at every offset and then interpolate the ray field to the source and receiver locations.

Both options require significant additional ray-tracing in 2-D, and even more in 3-D. We are always faced with the tradeoff of how much should we interpolate the rays versus how many additional rays should we shoot. In addition handling triplications of the wavefield can prove daunting.

With the moveout errors in terms of angle we only need to shoot a single ray-pair up from the imaging point at the angle α and β,

$$\begin{aligned} \alpha &= \phi + \theta \\ \beta &= \phi - \theta \end{aligned} \tag{1.31}$$

where θ is one-half the aperture angle, ϕ is the geologic dip (Figure 1.17). If the rays emerge at surface locations corresponding to an offset and CMP location inside the acquisition geometry we have a valid ray pair.

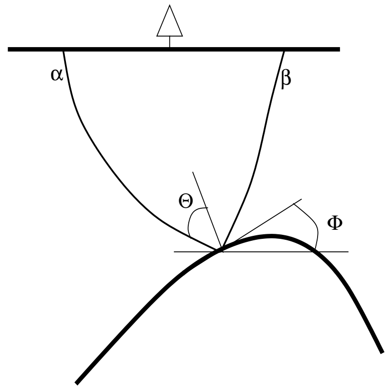

Figure 1.17: How the takeoff angle for a ray-pair are defined. tau-sketch [NR]

COMPARING DEPTH AND TAU TOMOGRAPHY

Now that I have set up the tomography problem it is time to test the theory and compare the advantage of depth vs. tau tomography. The model, Figure 1.3, is a difficult challenge for tomography, especially ray based tomography. The linearization approximation works best when we are close to the correct model. In this case the initial estimate is up to 1 km/s off in places. In ray tomography we assume that are raypaths are generally correct. With this model the initial reflector positions are in significant error. As a result we can't expect to get a satisfactory result after a single iteration of tomography,

Figure 1.18 is the result of migrating with the $s(z)$ slowness model (Figure 1.4). The correct reflector positions indicated with '*'. As expected, away from the anticline the gathers are flat and we have correctly positioned the reflectors. Along the edge of the anticline we see upward curvature in the CRP gathers indicating that I have used too slow a velocity at this location. Below the center of the anticline, $x = 10$, the bottom reflector shows some reverse moveout, the well known W pattern, better illustrated in Figure 1.15.

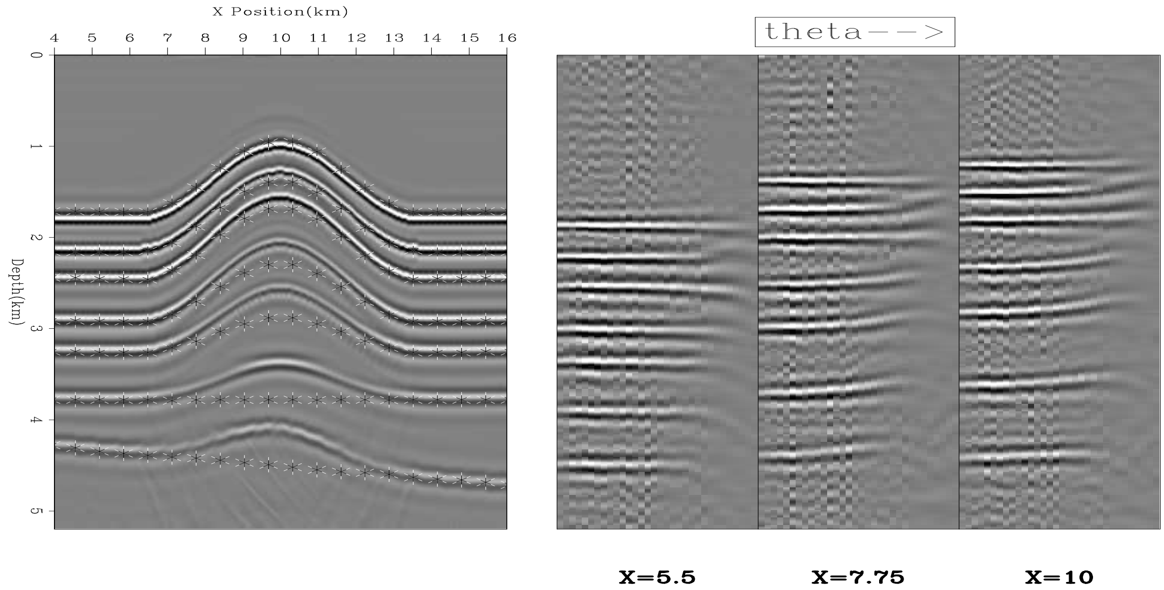

Figure 1.18: The initial migration result using a $v(z)$ velocity function from the edge of the anomaly. Right are three (z, θ) planes at different x postions. Note that the CRP gather at 5.5 is flat while the other two CRP gathers show significant moveout. tau-res.vel0 [ER]

First iteration

For the first comparison I applied a single non-linear iteration of depth (fitting goal 1.12) and tau (fitting goal 1.25), tomography. Figure 1.19 shows $\Delta\mathbf{s}$ and $\mathbf{v}$ for both. The $\Delta\mathbf{s}$ models are quite similar. The tau case has does a slightly better job finding the edges of the anticline. On the other hand the tau velocity model has an interesting artifact (the low velocity layer curving down) due to introducing the slowness change in tau rather than depth and then mapping back.

If I then migrate with the two velocity models we get very similar results. Both results Figures 1.20 and 1.21 show significantly better placement of the reflectors than the initial migration result, Figure 1.18. The tau result has done a slightly better job positioning the

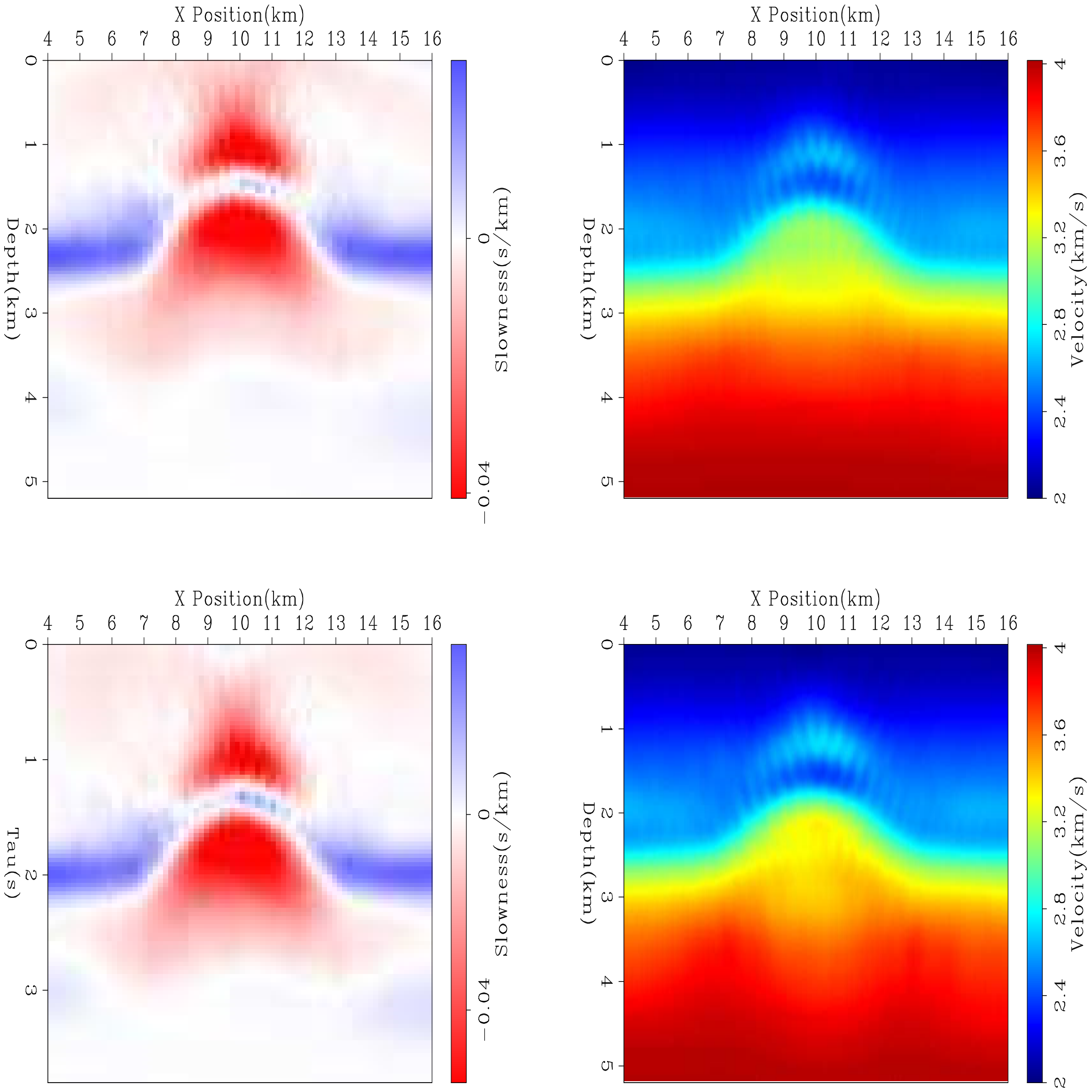

Figure 1.19: Slowness change (left) and velocity (right) after one iteration of depth (top) and tau (bottom) tomography. tau-iter1-comp [ER,M]

reflectors, especially within the anticline.

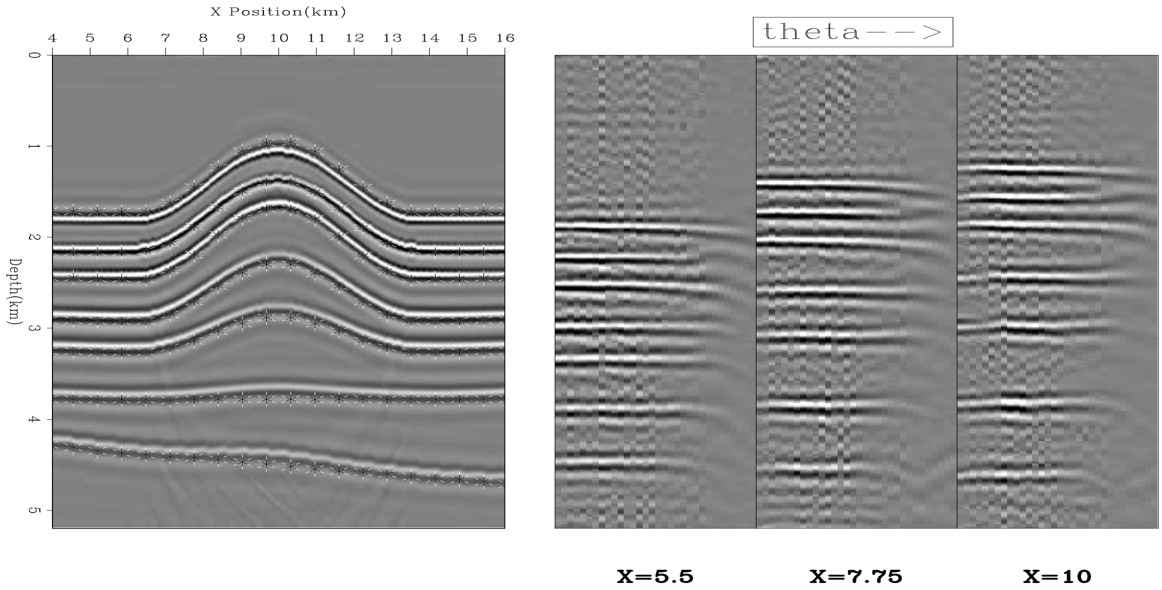

Figure 1.20: Migration result after one iteration of depth tomography. We have reduced the moveout and positioned the reflectors within the anticline significantly better than in Figure 1.18. tau-res.vel1.deltaz [ER,M]

Second iteration

With one more iteration of both depth and tau tomography the velocity model and the resulting depth migration improve. Figure 1.22 shows that for both depth and tau the anticline is better resolved. Both models show improvement in determining the low velocity layer and playing the dipping layers.

The advantage of performing the tomography in tau rather than depth has diminished. After a second iteration of tomography the migration results are virtually identical. Figure 1.23 shows the migration corresponding to the depth derived velocity model. The second iteration still shows some minor residual moveout in CRP gathers away from the anticline, but an overall improved positioning of the reflector.

Figure 1.24 shows the migration result after two iterations of tau tomography. Resolving the low velocity layer has allowed for better positioning of the upper reflectors. The lower

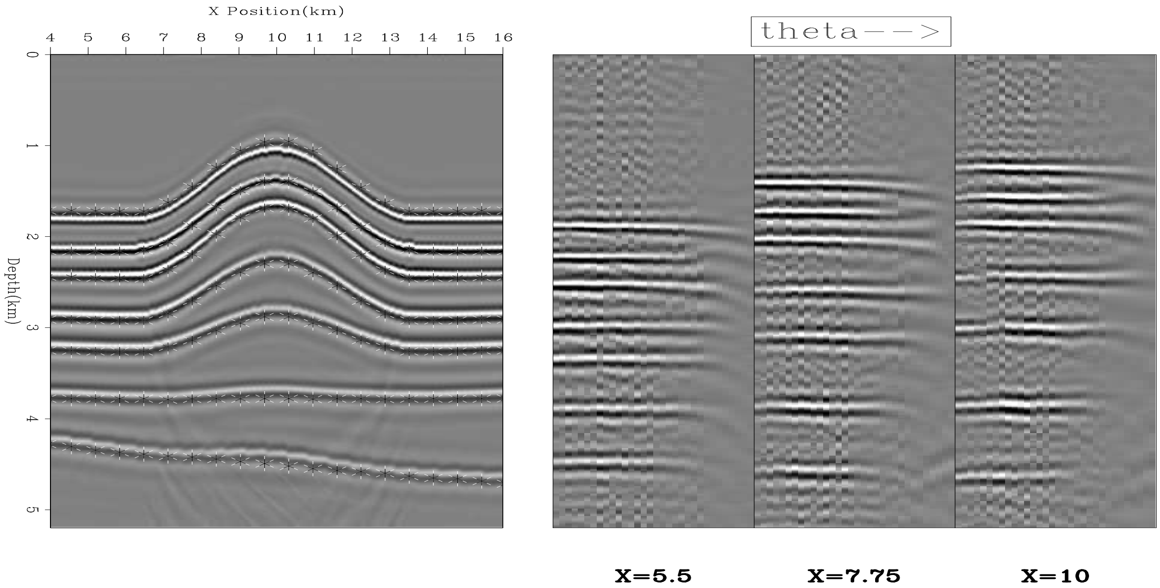

Figure 1.21: Migration result after one iteration of tau tomography. We have reduced the moveout and positioning errors compared to Figure 1.18. Positioning of all but the basement reflector is better than its depth counterpart, Figure 1.20. tau-res.vel1.deltatau [ER,M]

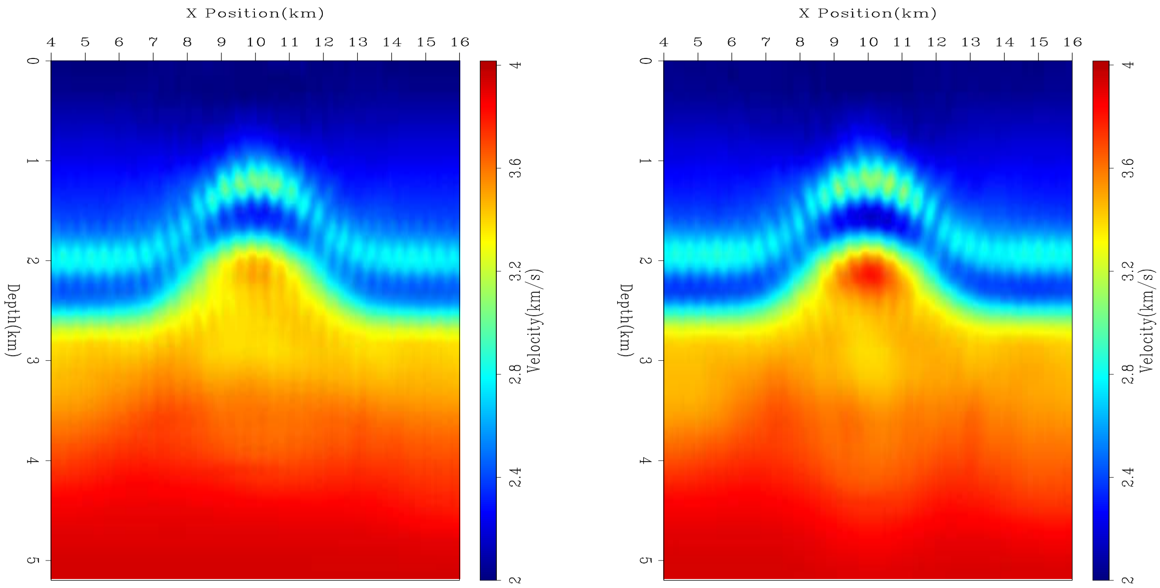

Figure 1.22: Velocity model after two iterations of depth (left) and tau (right) tomography. The tau results shows better isolation of the anticline and has even begun to resolve the low velocity layer. tau-iter2-comp-vel [CR,M]

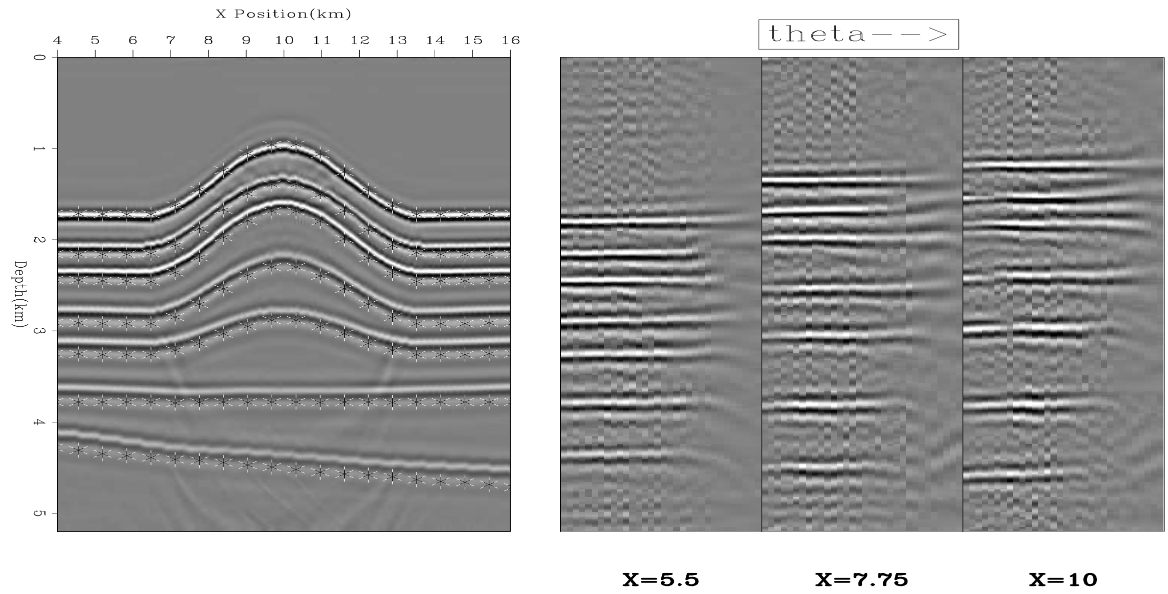

Figure 1.23: Migration result after two iterations of depth tomography. tau-res.vel2.deltaz [CR,M]

reflector's positioning and moveout is approximately the same as the depth result. Where we have the least amount of reliable information, the middle of the anticline, we have introduced slowness changes that are inconsistent with the idea of geology as a result positioning of the reflector isn't ideal.

Where to go from here?

Figure 1.25 show the semblance moveout measure (the initial semblance is shown in Figure 1.15) from the final tau migration, Figure 1.24. The semblance measures shows that we have virtually all of the moveout in the CRP gathers. The problem is that the updated velocity model (right panel of Figure 1.22) is not ideal. The largest error can be seen in the center of the anticline. We have introduced to high of a velocity directly below the low velocity layer, and compensated by introducing a lower velocity layer below that. In addition we have done a poor job in seeing the velocity contrast in the dipping layer. Generally our velocity model does not conform to our idea of geology. This is good focusing but unreasonable velocity model is often a bone of contention between processors and interpreters. The velocity model that best

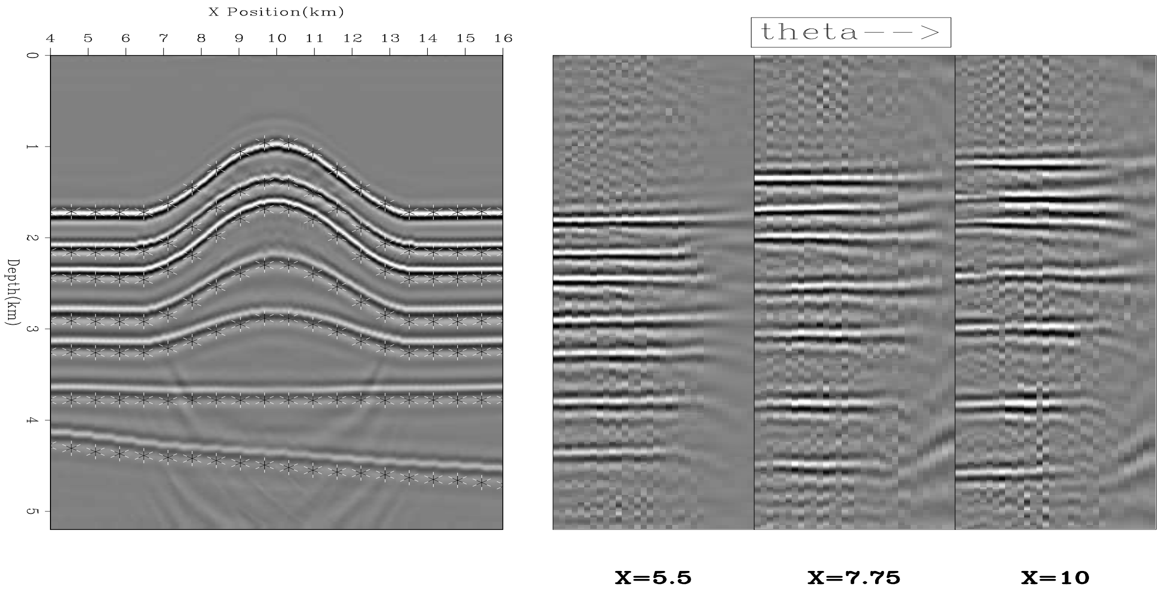

Figure 1.24: Migration result after two iterations of tau tomography. tau-res.vel2.deltatau [CR,M]

focuses the data often is not gelogically reasonable. In Chapter 3 I will address how we can reformulate the tomography problem so we obtain a velocity model that both flattens the CRP gathers and is geologically reasonable.

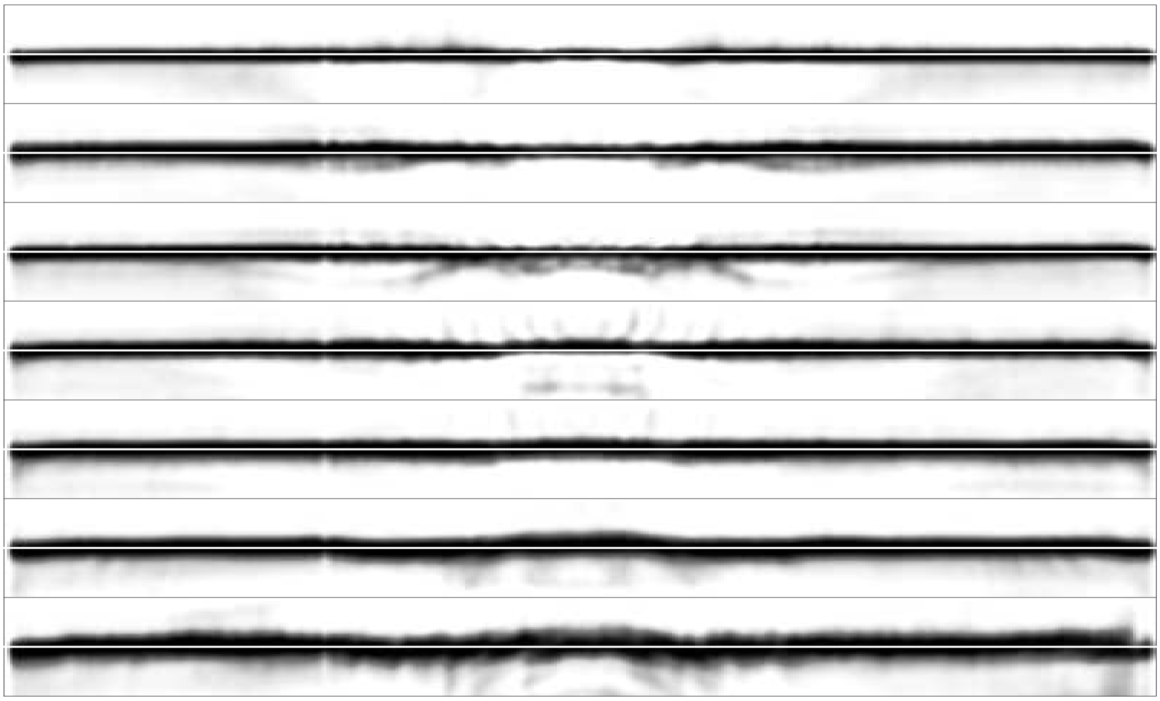

Figure 1.25: Moveout semblance measured at the seven reflectors on the tau tomography migration result, Figure 1.24. $\boxed{\text{tau-sem-final}}$ [CR,M]

Bibliography

Al-Chalabi, M., 1997, Parameter nonuniqueness in velocity versus depth functions: Geophysics, **62**, no. 03, 970–979.

Audebert, F., Nichols, D., Rekdal, T., Biondi, B., Lumley, D. E., and Urdaneta, H., 1997, Imaging complex geologic structure with single-arrival kirchhoff prestack depth migration: Geophysics, **62**, no. 05, 1533–1543.

Biondi, B., and Palacharla, G., 1996, 3-D prestack migration of common-azimuth data: Geophysics, **61**, no. 6, 1822–1832.

Biondi, B., Fomel, S., and Alkhalifah, T., 1997, "Focusing" eikonal equation and global tomography: SEP–**95**, 61–76.

Biondi, B., Fomel, S., and Chemingui, N., 1998a, Azimuth moveout for 3-D prestack imaging: Geophysics, **63**, no. 2, 574–588.

Biondi, B. L., Clapp, R. G., Fomel, S. B., and Alkhalifah, T. A., 1998b, Robust reflection tomography in the time domain: Robust reflection tomography in the time domain:, 68th Annual Internat. Mtg., Soc. Expl. Geophys., Expanded Abstracts, 1847–1850.

Biondi, B., Clapp, R. G., and Rickett, J., 1999, Testing linux multiprocessors for seismic imaging: SEP–**102**, 235–248.

Biondi, B., 1990, Velocity analysis using beam stacks: Ph.D. thesis, Stanford University.

Biondi, B. L., 1999, 3-D Seismic Imaging: Stanford Exploration Project.

Brown, M., 1998, Horizon refinement by synthesis of seismic and well log data: SEP–**97**, 193–206.

Carrion, P., 1991, Dual tomography for imaging complex structures: Geophysics, **56**, no. 9, 1395–1404.

Claerbout, J. Fundamentals of Geophysical Data Processing:. http://sepwww.stanford.edu/sep/prof/, 1976.

Claerbout, J. F., 1990, Nonlinear problems: SEP–**65**, 229–240.

Claerbout, J. F., 1992a, Earth Soundings Analysis: Processing versus Inversion: Blackwell Scientific Publications.

Claerbout, J. F., 1992b, Nonstationarity and conjugacy: Utilities for data patch work: SEP–**73**, 391–400.

Claerbout, J. Geophysical Estimation by Example: Environmental soundings image enhancement:. http://sepwww.stanford.edu/sep/prof/, 1998.

Claerbout, J. F., 1998b, Multi-dimensional recursive filtering via the helix: Geophysics, **63**, no. 5, 1532–1541.

Clapp, R. G., and Brown, M., 1999, Applying sep's latest tricks to the multiple suppression problem: SEP–**102**, 91–100.

Clapp, R. G., and Brown, M., 2000, $(t-x)$ domain, pattern-based multiple separation: SEP–**103**, 201–210.

Clapp, R. G., Fomel, S., and Claerbout, J., 1997, Solution steering with space-variant filters: SEP–**95**, 27–42.

Clapp, R. G., Sava, P., and Claerbout, J. F., 1998, Interval velocity estimation with a null-space: SEP–**97**, 147–156.

Clark, G. A., Glinsky, M. E., Devi, K. R. S., Robinson, J. H., Cheng, P. K. Z., and Ford, G. E., 1996, Automatic event picking in pre-stack migrated gathers using a probabilistic neural network: Automatic event picking in pre-stack migrated gathers using a probabilistic neural network:, 66th Annual Internat. Mtg., Soc. Expl. Geophys., Expanded Abstracts, 735–738.

Clayton, R. W., and Stolt, R. H., 1981, A born-wkbj inversion method for acoustic reflection data: Geophysics, **46**, no. 11, 1559–1567.

Crawley, S., 1998, Shot interpolation for Radon multiple suppression: 68th Ann. Internat. Meeting, Soc. Expl. Geophys., Expanded Abstracts, 1238–1241.

Crawley, S., 2000, Seismic trace interpolation with nonstationary prediction-error filters: SEP–**104**.

Delprat-Jannaud, F., and Lailly, P., 1992, What information on the earth model do reflection travel times provide?: J. Geophysical Research, **97**, 19827–19844.

Deutsch, C. V., and A.G., J., 1992, GSLIB: Geostatistical software library and user's guide: Oxford University Press.

Dix, C. H., 1955, Seismic velocities from surface measurements: Geophysics, **20**, no. 1, 68–86.

Ehinger, A., and Lailly, P., 1995, Velocity model determination by the SMART method, part 1: Theory: 65th Annual Internat. Mtg., Soc. Expl. Geophys., Expanded Abstracts, 739–742.

Etgen, J., 1990, Residual prestack migration and interval velocity estimation: Ph.D. thesis, Stanford University.

Fomel, S., and Claerbout, J. F., 1997, Exploring three-dimensional implicit wavefield extrapolation with the helix transform: SEP–**95**, 43–60.

Fomel, S., Clapp, R., and Claerbout, J., 1997, Missing data interpolation by recursive filter preconditioning: SEP–**95**, 15–25.

Fomel, S., 1997, A variational formulation of the fast marching eikonal solver: SEP–**95**, 127–147.

Fomel, S., 1999, Plane wave prediction in 3-D: SEP–**102**, 101–110.

Gazdag, J., and Sguazzero, P., 1985, Migration of seismic data by phase shift plus interpolation, *in* Gardner, G. H. F., Ed., Migration of seismic data: Society Of Exploration Geophysicists, 323–330.

Hale, I. D., 1983, Dip moveout by Fourier transform: Ph.D. thesis, Stanford University.

Hanson, D. W., and Witney, S. A., 1995, 3-D prestack depth migration – velocity model building and case history: 1995 Spring Symposium of the Geophys. Soc. of Tulsa, Soc. Expl. Geophys., Seismic Depth Estimation, 27–52.

Harlan, W. S., 1995, Regularization by model reparameterization: http://www.billharlan.com/pub/papers/regularization.pdf.

Harlan, W. S., 1996, Promising research topics: http://sepwww.stanford.edu/oldsep/harlan/papers/seg96review.ps.gz.

Hirsche, K., Porter-Hirsche, J., Mewhort, L., and Davis, R., 1997, The use and abuse of geostatistics: The Leading Edge, **16**, no. 03, 253–260.

Hubral, P., 1977, Time migration - some ray theoretical aspects: Geophys. Prosp., **25**, no. 4, 738–745.

Isaaks, E. H., and Srivastava, R. M., 1989, An Introduction to Applied Geostatistics: Oxford University Press.

Jacobs, J. A. C., Delprat-Jannaud, F., Ehinger, A., and Lailly, P., 1992, Sequential migration-aided reflection tomography: A tool for imaging complex structures: 62nd Annual Internat. Mtg., Soc. Expl. Geophys., Expanded Abstracts, 1054–1057.

Ji, J., 1997, Tomographic velocity estimation with plane-wave synthesis: Geophysics, **62**, no. 6, 1825–1838.

Kaipio, J. P., Kolehmainen, V., Vauhkonen, M., and Somersalo, E., 1999, Inverse problems with structural priorir information: Inverse Problems, **15**, 713–729.

Kosloff, D., Sherwood, J., Koren, Z., Machet, E., and Falkovitz, Y., 1996, Velocity and interface depth determination by tomography of depth migrated gathers: 61, **5**, no. 1511-1523.

Larner, K. L., Hatton, L., Gibson, B. S., and Hsu, I. C., 1981, Depth migration of imaged time sections: Geophysics, **46**, no. 5, 734–750.

Malcotti, H., and Biondi, B., 1998, Accurate linear interpolation in the extended split-step migration: SEP–**97**, 61–72.

Michelena, R. J., and Harris, J. M., 1991, Tomographic traveltime inversion using natural pixels: Geophysics, **56**, no. 5, 635–653.

Mosher, C. C., Foster, D. J., and Hassanzadeh, S., 1997, Common angle imaging with offset plane waves: 67th Annual Internat. Mtg., Soc. Expl. Geophys., Expanded Abstracts, 1379–1382.

Ottolini, R., and Claerbout, J. F., 1984, The migration of common-midpoint slant stacks: Geophysics, **49**, no. 3, 237–249.

Ottolini, R., 1982, Migration of reflection seismic data in angle-midpoint coordinates: Ph.D. thesis, Stanford University.

Podvin, P., and Lecomte, I., 1991, Finite difference computation of traveltimes in very contrasted velocity models: A massively parallel approach and its associated tools: Geophysical Journal International, **105**, 271–284.

Polak, E., 1997, Optimization: Algorithms and consistent approximations: Springer-Verlag, New York.

Prucha, M. L., Clapp, R. G., and Biondi, B. L., 1998, Imaging under the edges of salt bodies: Analysis of an Elf North Sea dataset: SEP–**97**, 35–44.

Prucha, M. L., Biondi, B. L., and Symes, W. W., 1999, Angle-domain common image gathers by wave-equation migration: Angle-domain common image gathers by wave-equation migration:, 69th Annual Internat. Mtg., Soc. Expl. Geophys., Expanded Abstracts, 824–827.

Prucha, M. L., Clapp, R. G., and Biondi, B., 2000, Seismic image regularization in the reflection angle domain: SEP–**103**, 109–119.

Ristow, D., and Ruhl, T., 1993, Extended split-step migration by cascading phase shift and finite difference operators: Extended split-step migration by cascading phase shift and finite difference operators:, Society Of Exploration Geophysicists, Annual Meeting Abstracts, 986–989.

Ronen, J., 1985, Multichannel inversion in reflection seismology: SEP–**46**.

Rowbotham, P. S., and Pratt, R. G., 1997, Improved inversion through use of the null space: Geophysics, **62**, no. 3, 869–883.

Sava, P., and Biondi, B., 1997, Multivalued traveltime interpolation: SEP–**95**, 115–126.

Sava, P., and Fomel, S., 2000, Angle-gathers by Fourier Transform: SEP–**103**, 119–130.

Stork, C., and Clayton, R. W., 1991, An implementation of tomographic velocity analysis: Geophysics, **56**, no. 4, 483–495.

Stork, C., 1992, Reflection tomography in the postmigrated domain: Geophysics, **57**, no. 5, 680–692.

Stork, C., 1994, Demonstration of mva tomography with controls and constraints for determining an accurate velocity model for prestack depth migration: 64th Annual Internat. Mtg., Soc. Expl. Geophys., Expanded Abstracts, 1338–1342.

Tarantola, A., 1987, Inverse problem theory: Elsevier.

Tieman, H. J., 1995, Migration velocity analysis: Accounting for the effects of lateral velocity variations: Geophysics, **60**, no. 01, 164–175.

Tikhonov, A. N., and Arsenin, V. Y., 1977, Solution of ill-posed problems: John Wiley and Sons.

Vaillant, L., and Biondi, B., 2000, Accuracy of common-azimuth migration approximations: SEP–**103**, 157–168.

Vaillant, L., and Calandra, H., 2000, Common-azimuth migration and Kirchhoff migration for 3-D prestack imaging: A comparison on North Sea data: SEP–**103**, 139–147.

Vaillant, L., and Sava, P., 1999, Common-azimuth migration of a North Sea dataset: SEP–**102**, 1–14.

van Trier, J., and Symes, W. W., 1991, Upwind finite-difference calculation of traveltimes: Geophysics, **56**, no. 6, 812–821.

van Trier, J., 1990, Tomographic determination of structural velocities from depth migrated seismic data: Ph.D. thesis, Stanford University.

Vidale, J. E., 1990, Finite-difference calculation of traveltimes in three dimensions: Geophysics, **55**, no. 5, 521–526.